Journal of Cleaner Production 240 (2019) 118124

Contents lists available at ScienceDirect

Journal of Cleaner Production

journal homepage: www.elsevier.com/locate/jclepro

Development and properties evaluation of sustainable ultra-high performance pastes with quaternary blends

P.P. Li [a, 1], Y.Y.Y. Cao [a, 1], H.J.H. Brouwers [a, b], W. Chen [b, **], Q.L. Yu [a, c, *]

[a] Department of the Built Environment, Eindhoven University of Technology, P.O. Box 513, 5600, MB Eindhoven, the Netherlands
[b] State Key Laboratory of Silicate Materials for Architectures, Wuhan University of Technology, Wuhan, 430070, PR China
[c] School of Civil Engineering, Wuhan University, Wuhan, 430072, PR China

ARTICLE INFO

Article history:
Received 15 May 2019
Received in revised form
16 August 2019
Accepted 20 August 2019
Available online 21 August 2019

Handling editor: Baoshan Huang

Keywords:
Ultra-high performance concrete
Environmental sustainability
Quaternary binder
Synergistic effect

ABSTRACT

This study aims to investigate the synergistic effect of quaternary blends applying supplementary cementitious materials on sustainable Ultra-high Performance Concrete (UHPC) pastes. The hydration kinetics, pore structures, fresh behaviour, strength, fibre-to-matrix bond, shrinkage and environmental sustainability of 14 UHPC pastes are determined and analysed. The results show that limestone powder contributes to better environmental sustainability and fresh behaviour, but enlarged shrinkage and diminished strength, and application of silica powder is an effective measure to overcome those disadvantages. Slag cement possessing a relatively lower Ca/Si ratio (2.45) is preferred to a lower amount but finer silica (3% nano silica) in the presence of limestone powder, compared to the Portland cement with a higher Ca/Si (3.22) that needs more silica even with coarser particle size (5% micro silica). Quaternary blends with cement-slag-limestone-silica in UHPC pastes have considerable advantage of reducing embedded CO_2 emission and and improving sustainability efficiency. Furthermore, positive synergies in term of strength, fibre-to-matrix bond and total free shrinkage are observed in UHPC pastes with quaternary binders compared to binary and ternary ones.

1. Introduction

Ultra-high Performance Concrete (UHPC) has received great attention in the concrete industry, thanks to its superior properties including fresh behaviour, mechanical properties, durability and energy absorption (Li and Yu, 2019; Su et al., 2017; Wang et al., 2014). Although the structures made by UHPC are sustainable when considering the lower concrete demand and longer service life due to the higher strength and better durability, the binder or cement consumption in UHPC itself is often more than 900 kg/m^3, e.g. 37.9% by the total mass as illustrated in Fig. 1 (Stengel and Schießl, 2014), which is approximately three times as that in normal strength concrete (Zhong et al., 2018). The high binder utilization certainly causes more cost, energy consumption and embedded CO_2 emission problem, and consequently limits a wider engineering application of UHPC.

The cement products occupy 5% CO_2 emissions of the total global output and 4600 MJ/ton energy consumption (Hendriks et al., 2002; Vance et al., 2013). To decline the environmental impact of Portland cement concrete, substituting cement by suitable supplementary cementitious materials (SCMs), e.g. fly ash, slag, glass powder and silica fume, has been studied (Colangelo et al., 2017; Crossin, 2015; De Belie et al., 2010; Sharma and Khan, 2017). The ground granulated blast furnace slag has shown as a promising material (Gholampour and Ozbakkaloglu, 2017; Yu et al., 2017), due to its much lower embedded CO_2 emission and better durability than those of cement, as an industrial by-product (Crossin, 2015; King, 2012; Mo et al., 2016). As a natural resource on earth, limestone powder is more sustainable because of the abundant reserve and low embedded CO_2 emission during production process. Furthermore, very low water-to-cement ratios are normally used in UHPC to reduce the porosity and enhance the strength, which causes a large amount of incompletely hydrated cement grains in UHPC (Yu et al., 2014a). Therefore, it is reasonable to replace certain amount of cement by unreactive powder such as limestone powder as filler to improve the environmental and economical sustainability benefits. However, the addition of limestone powder tends to decrease the strength and durability of UHPC, because of the dilution effect (Yu et al., 2015). Pozzolanic

* Corresponding author. School of Civil Engineering, Wuhan University, Wuhan, 430072, PR China.
** Corresponding author.
E-mail addresses: chen.wei@whut.edu.cn (W. Chen), q.yu@bwk.tue.nl (Q.L. Yu).
[1] Equivalent first authors.

https://doi.org/10.1016/j.jclepro.2019.118124
0959-6526/

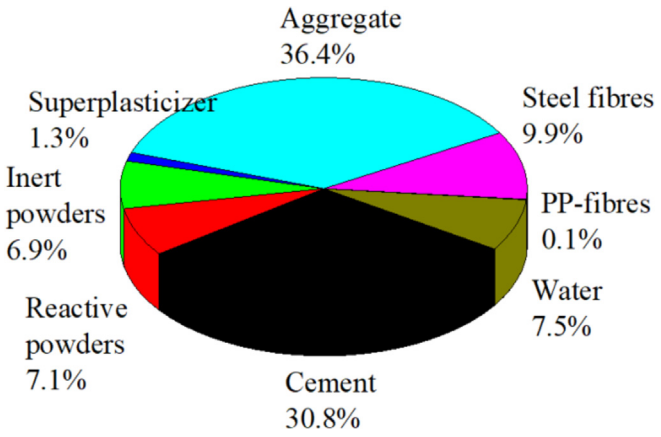

Fig. 1. Average composition of UHPC from 75 references (Stengel and Schießl, 2014).

materials, such as micro silica and nano silica, could probably overcome those disadvantages by the effects of nucleation and filling, and pozzolanic reaction (Nili and Ehsani, 2015; Pedro et al., 2017). As illustrated above, slag, limestone and silica powder have their special advantages and are suitable to develop sustainable UHPC.

However, current researches on developing sustainable UHPC through substituting Portland cement by the mentioned SCMs are mainly concentrating on binary and ternary blends (Edwin et al., 2019, 2016; Koutný et al., 2018; Shi et al., 2015). Positive synergistic effects of ternary binder with cement-silica fume-slag has been demonstrated on workability and early-age strength due to the accelerated hydration by silica fume and low water demand of slag, but shows negative synergistic effects on porosity and later-age strength because of dilution effect (Shi et al., 2015). It showed that ternary binder with cement-silica-limestone has great potential to benefit sustainability and strength of UHPC mixtures by replacing some cement and silica powder, because of pozzolanic effect of silica, and filler effect and high sustainability of limestone powder (Burroughs et al., 2017). Several researchers also reported benefits of quaternary binders in ordinary mortar and concrete, such as positive effect on strength and chloride resistance with cement-fly ash-silica fume-metakaolin/slag/limestone by optimum composition combination (Dave et al., 2017, 2016); good sulfuric acid resistance under drying-immersion cycles with cement-slag-limestone-pozzolana by reducing portlandite and degradation of hydrated compounds of cement, attributed to the dilution effect of limestone and pozzolanic reactions by slag and pozzolana (Makhloufi et al., 2016, 2014), improvement on shrinkage and permeability in hot climate with cement-fly ash-slag-silica fume by accelerating the hydration process (El-chabib and Ibrahim, 2013). Nevertheless, there is no study yet on quaternary system by adding cement-slag-limestone-micro/nano silica in UHPC. The probable positive or negative synergy of quaternary binder with cement-slag-limestone-silica is not clear in the special system of UHPC characterized with low water and high superplasticizer amount. In addition, most of the studies on environmental sustainability evaluation of concrete applying supplementary cementitious materials were performed by comparing only one or two materials (Van den Heede and De Belie, 2014) and a sound analysis of whole binding materials on environmental sustainability is of highly significance.

This study aims to understand the synergistic effect of quaternary binders with cement-slag-limestone-micro/nano silica in developing sustainable UHPC pastes. The hydration kinetics, pore structure, fresh behaviour, compressive strength, fibre-to-matrix bond, total free shrinkage of sustainable UHPC pastes are evaluated. Then, the embedded CO_2 emission and sustainability efficiency of the designed UHPC pastes based on performance are analysed and discussed. Furthermore, the positive synergies in terms of strength, bond and shrinkage are assessed to demonstrate the reasonability of quaternary blends in sustainable UHPC instead of binary or ternary ones.

2. Experimental program

2.1. Materials

Several initial materials are used, including cement CEM I 52.5 R (PC), ground granulated blast furnace slag (GGBS) cement CEM III/A 52.5 N (SC) with 50% of slag by mass, limestone powder (LP), densified micro-silica from Elkem Grade 920E D (mS), aqueous dispersion of colloidal nano-silica (nS), water, polycarboxylic ether based superplasticizer (SP). Both Portland cement and slag cement are from the same manufacturer (ENCI), and slag cement is chosen as binary binder considering its already optimized particle size distribution and homogeneous mixing during the manufacture instead of blending GGBS into the Portland cement by ourselves. The particle size distributions of powders are shown in Fig. 2, except for mS due to the densified process makes it difficult to be measured. A 3D hook ended steel fibre (Dramix RC-80/30-BP) is used to research the fibre-to-matrix bonding effect by single fibre pull-out test. Table 1 shows the chemical and physical properties of powders, respectively.

2.2. Mix proportion

A total of 14 pastes with a low water-to-powder ratio of 0.2 are produced to simulate the UHPC system, and the water-to-powder ratio is chosen based on the previous research (Li et al., 2018; P. P. Li et al., 2017a). The pure PC is applied as the reference binder, while the remaining binders are binary (SC), ternary (PC + mS/nS + LP) and quaternary (SC + mS/nS + LP) cementitious blends. The SC contains 50% GGBS which is therefore regarded as binary binder. The replacement levels for LP are 10%, 20% and 30% by the total mass of powders, while those of mS and nS are 5% and 3%, respectively, based on the previous studies (Li et al., 2018; Yu et al., 2014b). The difference between the dosage of nano-silica and micro-silica is caused by the higher pozzolanic, filler and nucleation effects with clearly finer particle size and larger specific surface area of nano-silica. In addition, excessive nano-silica addition

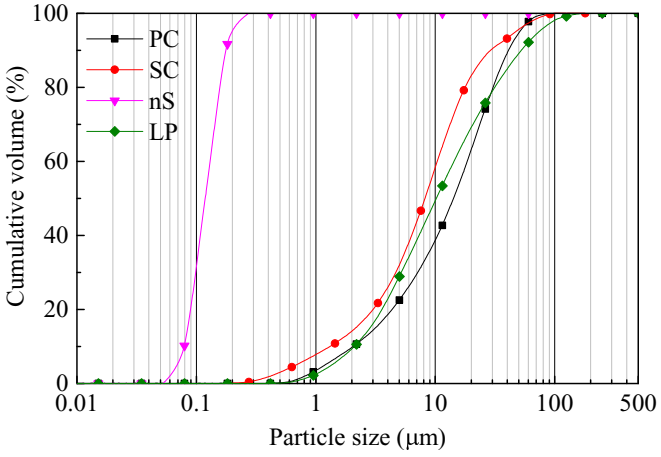

Fig. 2. Particle size distribution of powders.

Table 1
Chemical and physical properties of the PC, SC, ms, nS, LP.

Substituent (%)	PC	SC	mS	nS	LP
CaO	64.60	54.54	0.90	0.08	97.21
SiO_2	20.08	22.27	93.06	98.68	0.87
Al_2O_3	4.98	7.64	–	0.37	0.17
Fe_2O_3	3.24	1.61	2.06	–	0.13
K_2O	0.53	0.42	1.15	0.35	–
Na_2O	0.27	–	0.63	0.32	–
SO_3	3.13	5.52	1.28	–	0.11
MgO	1.98	5.35	0.70	–	1.17
TiO_2	0.30	0.83	–	0.01	0.01
MnO	0.10	0.19	0.07	–	0.01
Specific density (g/cm^3)	3.15	3.03	2.32	2.22	2.71
BET surface area (m^2/kg)	1420	1590	18400	22700	1080

would cause significant issues on water demand and resulting workability. A polycarboxylic ether type superplasticizer (SP) with a solid content of 35% is applied with a fixed content (1% by mass of powders) to adjust the flowability of the mixtures. The mixture proportions are summarized in Table 2. The mixing procedure of UHPC pastes is illustrated in Fig. 3. For hardened properties assessment, samples are cast and domolded after 24 h and then cured in water under ambient conditions (20 ± 1 °C) till the testing age.

2.3. Experimental program

2.3.1. Isothermal calorimetry

An isothermal calorimeter is used to research the effect of quaternary blends on the hydration kinetics by setting the temperature of 20 °C (TAM Air, Thermometric). The ready mixed pastes are filled into an ampoule and immediately loaded into the calorimeter. The heat flow is measured continuously for approximately 7 days.

2.3.2. Mercury intrusion porosimetry

The pore size distributions of the hardened pastes are measured by mercury intrusion porosimetry (MIP, Micromeritics AutoPore IV) after 56 days water curing. The hardened pastes are crushed into small pieces of 2–4 mm, and approximately 1.5 g dried samples are used for measurement. The intrusion pressure changed from 0 to 227 MPa, with an Hg surface tension of 485 dyn/cm and contact angle of 130°.

2.3.3. Fresh properties

The consistency of UHPC paste is described by spread flow in conformity with the EFNARC specification (EFNARC, 2005). The spread flow is tested by using the mini truncated conical cone without jolting, at ambient temperature of 20 ± 2 °C. Meanwhile, the fresh paste is filled in a container with a known volume to determine its fresh density ρ. Most packing densities are measured under dry condition based on codified test methods (EN-1097-3, 1998; Li and Kwan, 2014), which cannot reflect the real compactness in the real wet condition, especially in the presence of superplasticizer in UHPC. In order to research the compactness under real wet condition, a wet packing density is proposed and described by the solid concentration (Li and Kwan, 2014), as,

$$\phi = \frac{V_{solid}}{V_{container}} = \frac{\sum_i^n \frac{r_i}{\rho_i} m \frac{1}{(1+w/p)}}{V_{container}} = \sum_i^n \frac{r_i}{\rho_i} \frac{\rho}{(1+w/p)} \quad (1)$$

where ϕ is the wet packing density, V_{solid} is the solid volume of the particles, $V_{container}$ is the volume of testing container (bulk volume of mixture), m is the mass of paste, r_i and ρ_i are the mass fraction and density of powder i, w/p is the water-to-powder ratio as 0.2 in this study.

2.3.4. Compressive strength

The compressive strength of hardened UHPC paste is tested by cubic specimens with a size of 50 mm × 50 mm × 50 mm after 28 days and 56 days, following EN 12390 (EN 12390-3, 2009). The fresh pastes are poured in steel moulds and covered with plastic film to keep moisture. After 24 h, the hardened specimens are demoulded, following with the water curing under temperature of 20 ± 1 °C.

2.3.5. Fibre-to-matrix bond

Dog-bone shape moulds following the standard ASTM C307-03 (C 307-03, 2004) are used to cast the specimens for carrying out the steel fibre pull-out tests. A piece of hard foam is put in the middle of the mould, separating the mould into two parts. A half-length embedded hooked-end steel fibre is held by the hard foam in Fig. 4 (a), then the fresh paste is poured into one half of the mould, shown in Fig. 4 (b). Similar curing regime is applied as shown in Section 2.3.4. The pull-out tests are performed after 56 days, under the displacement control (0.5 mm/min) with a 30 kN load cell, illustrated in Fig. 4 (c).

2.3.6. Total free shrinkage

The total free shrinkages are measured based on prism specimens (40 mm × 40 mm × 160 mm), following DIN 52450-A (DIN 52-450, 1985). The fresh pastes were first covered by plastic film for 24 h, then demoulded and cured in a condition with a relative humidity (RH) of 50% at 20 ± 1 °C. The demoulding time (24 h) is regarded as the "zero time", and the changed length is recorded periodically for a duration of 91 days, by employing a length comparator with a measurement accuracy of 0.001 mm.

Table 2
Mix proportions of UHPC pastes (w/p = 0.2, SP 1%).

Mix	Note	PC (%)	SC (%)	mS (%)	nS (%)	LP (%)
M1	PC	100	–	–	–	–
M2	PC5mS10LP	85	–	5	–	10
M3	PC5mS20LP	75	–	5	–	20
M4	PC5mS30LP	65	–	5	–	30
M5	PC3nS20LP	87	–	–	3	10
M6	PC3nS20LP	77	–	–	3	20
M7	PC3nS20LP	67	–	–	3	30
M8	SC	–	100	–	–	–
M9	SC5mS10LP	–	85	5	–	10
M10	SC5mS20LP	–	75	5	–	20
M11	SC5mS30LP	–	65	5	–	30
M12	SC3nS20LP	–	87	–	3	10
M13	SC3nS20LP	–	77	–	3	20
M14	SC3nS20LP	–	67	–	3	30

3. Results and discussion

3.1. Hydration kinetics and pore structures

Fig. 5 shows the influence of different blends on the hydration kinetics of UHPC pastes. The heat flow is characterized by the time to reach the maximum peak (TRMP) and the maximum heat flow (MHF). The pure PC paste has the longest TRMP (17 h) and highest MHF (3.7 mW/g). More LP addition shows a slightly faster hydration but lower normalized heat flow and normalized total heat when comparing the mixtures of M2 and M4, which indicates that LP addition mainly shows dilution effect on the cement clinker, but as well as somewhat acceleration effect due to nucleation sites for

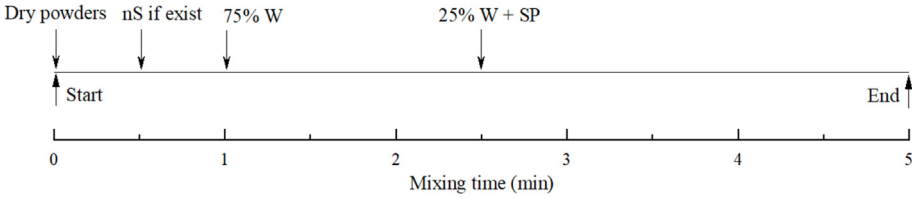

Fig. 3. Mixing procedure of mixtures.

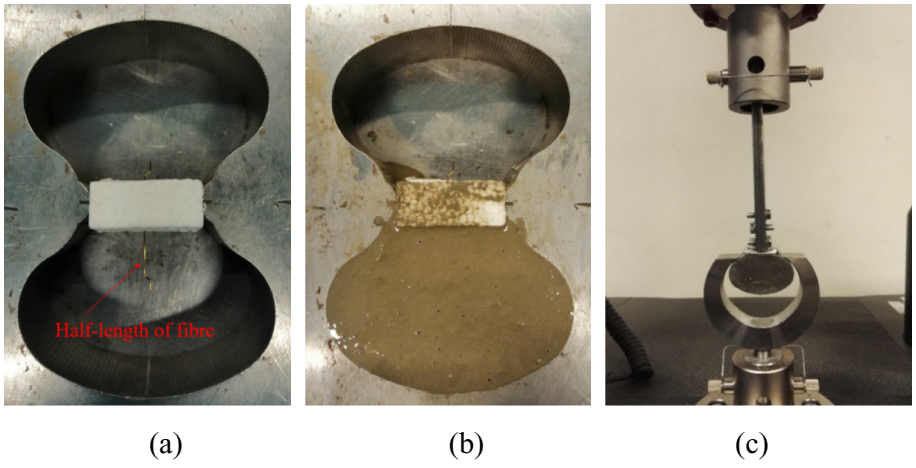

Fig. 4. (a) Fixed steel fibre, (b) sample and (c) set-up for fibre pull-out test.

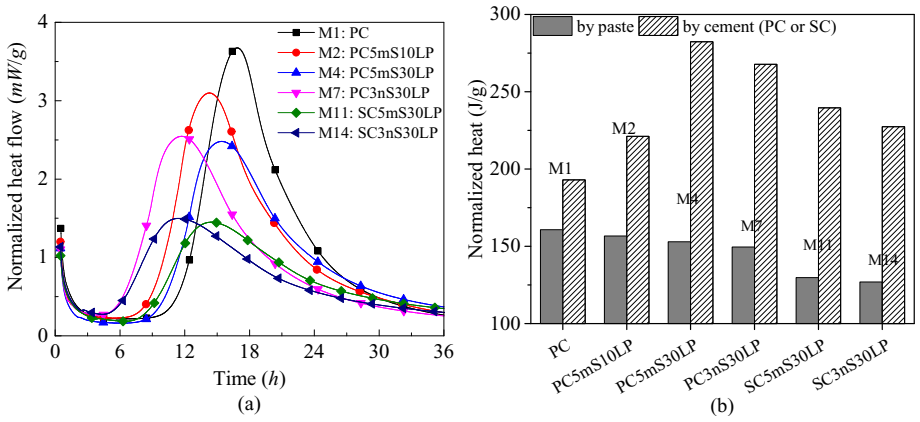

Fig. 5. (a) Normalized heat flow and (b) normalized heat.

hydration products. While, the normalized total heat by cement before the 7 days of M4 is much larger than that of M2, which means the hydration degree of cement can be improved with more LP addition. The mixtures of M7 and M14 show much earlier TRMP compared to the M4 and M11, which is attributed to the higher surface area and increased number of nucleation sites by 3% nS than the 5% mS. The GGBS in SC further enlarges the dilution effect on hydration, as confirmed by the much lower normalized heat flow and total heat of M11 and M14 compared to the M4 and M7.

Fig. 6 presents the pore size distribution of the designed hardened pastes after 56 days. This study mainly focuses on the pore sizes ranging from 5 nm to 100 nm, because the pore size distributions of all designed mixtures between 100 nm and 100 μm are very low and similar to each other. The critical pore diameters (the peak in the differential pore size distribution curve) of the designed mixtures range between 30 nm and 50 nm. With the inclusion of 5% mS and 10% LP in PC, the pore structure of M2 with ternary binder is densified compared to M1, especially for pore sizes between 30 nm and 60 nm. While, more addition of LP up to 30% (M4) results in a shift of the critical pore diameter to a smaller size and causes a large amount smaller pores, which is due to the dilution effect and generates low-density and porous C–S–H gel phases (Yajun and Cahyadi, 2003). When the PC is replaced by the SC, the pore size distribution of M11 with quaternary binder tends to a shift towards larger diameters and the pore volume is enlarged compared to M7 with ternary binder. While, the pore structure of mixture with quaternary binder can be considerably improved by using 3% nS instead of 5% mS, namely extending M11 to M14.

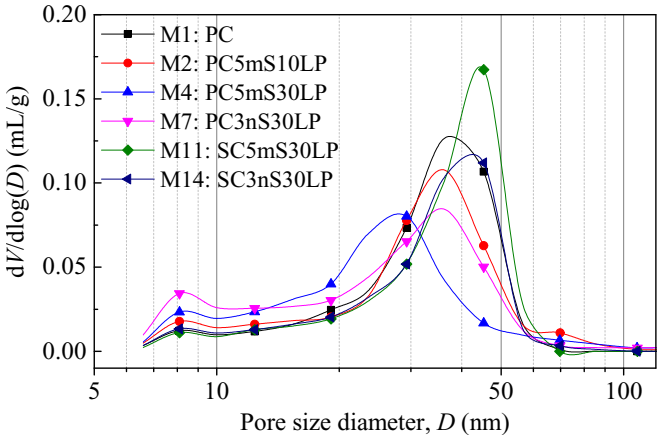

Fig. 6. Differential pore size distribution.

3.2. Fresh behaviour

The spread flow and wet packing density results are summarized in Fig. 7. According to our previous study, the PCE-type superplasticizer (SP) is one of the most important factors and has a great influence on the fresh behaviours of UHPC (Li et al., 2017a). Both water and superplasticizer contents have very important effect on the particle packing of matrix under real wet conditions (Li and Kwan, 2014). In this study, SP with a dosage of 1% can provide the system with an excellent workability and self-compacting characteristics, namely mini slump flow more than 35 mm. The excellent fresh behaviour is due to the adsorption of PCE molecules on particles and consequently dispersing the particles by mainly electrostatic repulsion and steric effect. Furthermore, our previous study confirmed that the saturation dosage of UHPC paste is around 1% with water-to-powder ratio of 0.2. The spread flow cannot be further improved beyond the saturation dosage (Li et al., 2017a).

The quaternary binder tends to possess large wet packing density, with a maximum value of 0.636 in the case of M14. Mixtures with Portland cement (M1) and Slag cement (M8) result in similar wet packing densities, around 0.617. LP contributes to an increased compactness, probably due to better fresh behaviour and particle size distribution. A good fresh behaviour means a sufficient free water to fill the voids in the bulk volume of the matrix that avoids entrapping air in the voids, which efficiently decreases the larger pores. Furthermore, it is hypothesized that cement incorporating limestone powder can optimized the total particle size distribution and increase the compactness compared to the pure cement (Arora et al., 2018; Burroughs et al., 2017). As seen in Fig. 7 and 3% nS leads to a better compactness than 5% mS under the same other conditions, because of its finer particle size and better filling effect.

The SC pastes (M8) have a slightly smaller spread flow compared to PC pastes (M1), 42.1 cm vs. 43.5 cm. It indicates that the SC shares similar overall integrated effects by water demand and adsorption ability of PCE-type superplasticizer as PC clinker. With the increase of LP from 10% to 30%, the spread flow of mixtures is improved significantly, e.g. 36 cm (M5) to 41.2 cm (M7). The LP is mainly composed of Ca^{2+} and CO_3^{2-} ions, which result in a neutral surface. In aqueous solution, the OH^- groups preferably concentrate on the Ca^{2+} surface, resulting in electrostatic repulsion between particles, which consequently improves the fluidity and decreases particle flocculation (Sekkal and Zaoui, 2013). Moreover, the lower water demand of LP than those of PC, GGBS and mS/nS benefits better fluidity of UHPC pastes (Domone and Hsi-wen, 1997; Li et al., 2018). Normally, the mS and nS have negative effects on the fresh behaviour of cementitious materials (Li et al., 2018; Yu et al., 2014b). They have quite high water demand and consume large amount of superplasticizer, leading to the reduction of effective lubricating water content between the particle voids (Schröfl et al., 2012). As seen in Fig. 7, the spread flow of pastes with nS is always worse than that of similar mixtures with mS, e.g. with spread flow from M2 of 45 cm to M5 of 36 cm, because of the higher fineness and pozzolanic effect, which enlarges the inter-particles friction (Lei et al., 2016).

3.3. Compressive strength

The compressive strength of UHPC pastes, measured after 28 days and 56 days, are shown in Fig. 8. At 28 days, the compressive strengths vary between 131.3 MPa and 153.8 MPa 20% LP addition to the system shows a positive contribution on the 28 days compressive strength of mixtures with PC. The strengths further increase up to the range from 137.2 MPa to 181.8 MPa, with the maximum strength at pure PC paste (M1), at the curing age of 56 days.

The mixtures without GGBS (M1~M7), but with the same

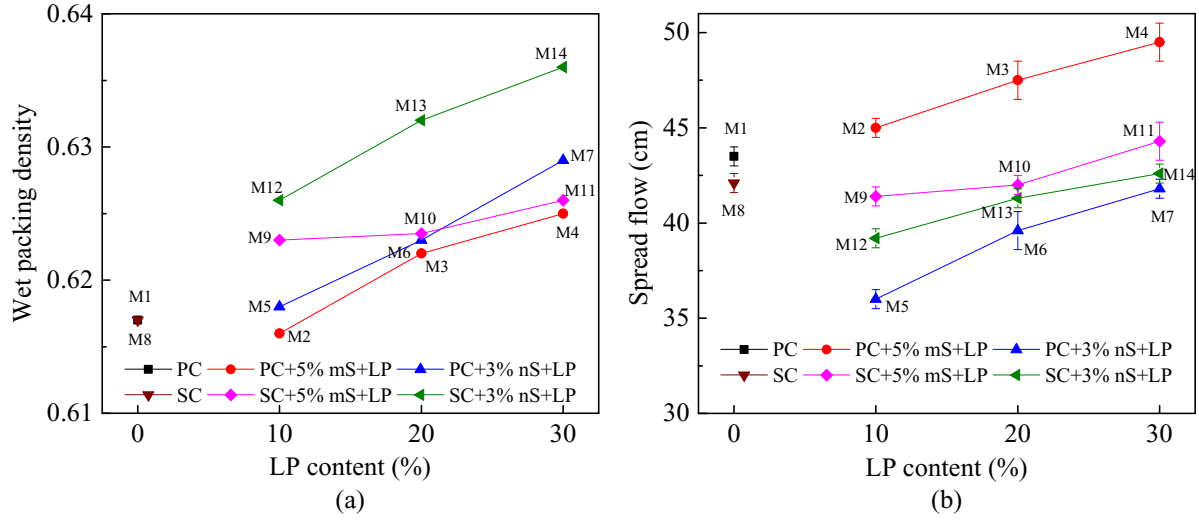

Fig. 7. Fresh behaviour of UHPC pastes.

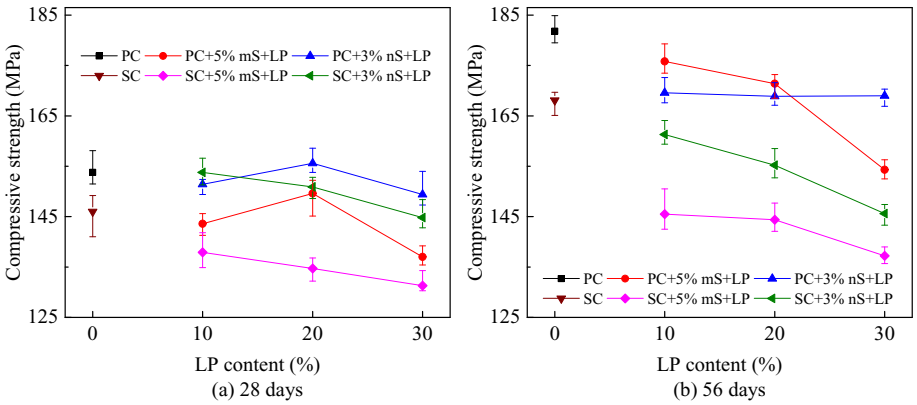

Fig. 8. Compressive strengths of UHPC pastes.

amount of mS/nS and LP, show slightly higher compressive strength than the mixtures with GGBS (M8~M14) at both 28 days and 56 days, which indicates that GGBS results in lower strength development potential for UHPC pastes. However, ordinary strength concrete incorporates GGBS often shows a better compressive strength at later age due to the formation of C–S–H by consuming portlandite, even for UHPC with GGBS substitution rate of 25% (Shi et al., 2015). When adding a high amount of GGBS in low water-to-binder system, such as 50% in this study, 30% and 60% in (Bouasker et al., 2014), 50% in (Shi et al., 2015), and 31% in (Yu et al., 2015), the later age (e.g. 56 or 90 days) strengths are lower than those of mixtures without GGBS. This is probably attributed to the low water amount and dilution effect (as seen in Fig. 5) of clinker by the high amount of GGBS, then the produced portlandite from PC and free water to solute portlandite are quite limited. Thus, no saturated calcium hydration solution can contact and activate the GGBS, which results in lower strength development potential at later age (Shi et al., 2015). Some researchers also attributed this phenomenon of lower later strength to the special UHPC system with a high superplasticizer content and low water amount (Yu et al., 2015), which might significantly affect the pozzolanic reaction and cause slow increase of strength development.

LP leads to lower compressive strength of UHPC paste due to dilution effect, leading to weaker bonding force and less hydration products, as confirmed in Fig. 5. But the decrease is quite limited in the presence of mS/nS in this study, especially for the ternary mixtures (M2~M7). Because LP also shows some benefits, such as increased water-to-clinker ratio and then enhanced hydration potential of reactive binder (as illustrated by the normalized heat by cement in Fig. 5(b)), enlarged nucleation sites for the hydration products of cement (Li et al., 2015), preferably generated more stable carboaluminate hydrate (Bentz et al., 2017; Kakali et al., 2000). In addition, the application of LP can also improve the flow ability and packing density under real wet condition, as illustrated in Section 3.2, which means decreased larger pores (Li and Kwan, 2014).

Due to the decrease of compressive strength by introducing LP and GGBS, it is wise to compensate it adding more reactive pozzolans such as mS and/or nS. Because mS and nS can strengthen the compressive strength of the mixtures attributed to their high pozzolanic effect on consuming $Ca(OH)_2$ to form C–S–H, filling internal pores with finer particle, and nucleation effect (Nili and Ehsani, 2015; Shi et al., 2015). In this paper, 5% mS and 3% nS are utilized by considering their efficiency (Li et al., 2018; Yu et al., 2014b) and agglomeration issue (Hosseini et al., 2011; Lei et al., 2016). Based on the results in Fig. 8 and 5% mS contributes higher strength than 3% nS for the mixtures containing PC, e.g. with compressive strength from M2 of 175.8 MPa to M5 of 169.6 MPa after 56 days. While this trend reverses for the mixture incorporating SC (M9~M14), e.g. with compressive strength from M9 of 145.5 MPa to M12 of 161.3 MPa after 56 days. This is probably due to two factors, namely different Ca/Si ratios with the different cementitious material blends and the different fineness of silica powders (Hong and Glasser, 2004). The appropriate Ca/Si ratio has been reported to be around 1.30 (Yazici et al., 2008). And both more silica amount (5%) and finer particle size (nS) are in favour of higher strength. Therefore, the PC with a higher Ca/Si ratio (3.22) needs more silica (5% mS) even coarser particle size, and the SC with a lower Ca/Si ratio (2.45) are preferred to a lower amount but more reactive and finer silica, i.e. better fineness (3% nS). It can be concluded that 5% mS is more effective on Portland cement for the ternary binders (PC-mS-LP), while 3% nS on slag cement for the quaternary (SC-nS-LP) binders.

3.4. Fibre-to-matrix bond characteristics

The fibre-to-matrix bond is also characterized in the present study considering the fact that steel fibres are usually utilized in the UHPC system. Therefore, the bonding behaviour contributes to the understanding of the investigated blended binders from the UHPC matrix point of view. Two different responses are observed during the fibre pull-out tests, namely, complete fibre pull-out and fibre breakage at the hood end, and the related two force-displacement curves are plotted in Fig. 9 (a). The curve representing the complete fibre pull-out procedure can be divided into five phases (Cao and Yu, 2018). In the initial phase P_1, the response of the curve is almost during elastic stage until fibre debonding. Thereafter, debonding phase P_2 takes place and the adhesion bond fails continuously. After the complete debonding of the fibre, anchorage phase P_3 is activated, during which bending of the hook occurs. Plastic hinges are formed due to the bending effects on the hook, inducing additional anchorage that significantly amplifies the pull-out force. As the pull-out process continues, the force reaches its maximum values, then the hook undergoes a straightening phase P_4. In the last phase (P_5), the fully straightened fibre slips along the tunnel, the pull-out behaviour of which is determined by the frictional force. The pull-out load reduces gradually with the decrease of the remained embedded length.

In the pull-out tests, fibre breakage occurs frequently thanks to the strong bond between the fibres and the designed UHPC pastes. Examples of the steel fibre before pull-out, after complete pull-out and experienced fibre breakage are illustrated in Fig. 9 (b). The fibre breaks at a location near the hook, which has more serious stress concentrations compared to the straight part of the fibre. The

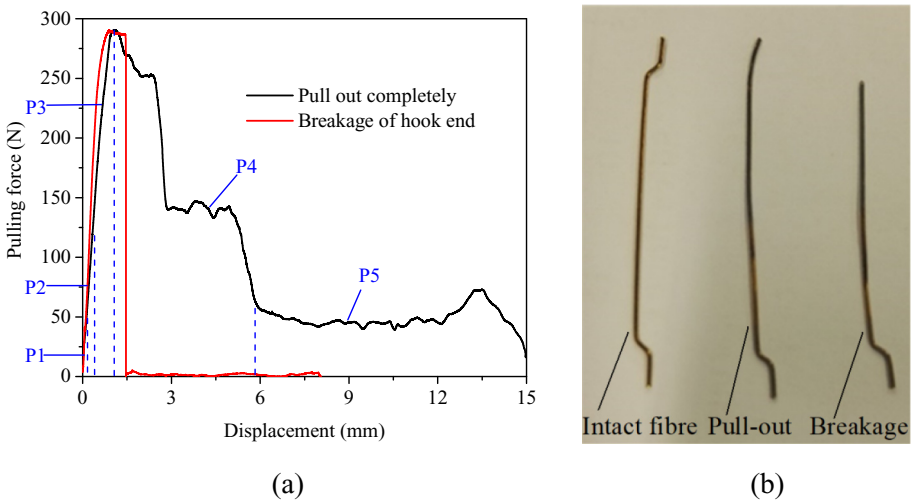

Fig. 9. Typical force-displacement curves (a) and failure patterns of steel fibre (b).

critical pull-out force for the fibre breakage is approximately 290–300 N in this study, which indicates the full utilization of the fibre tensile capacity. As suggested by Robins et al. (2002), the fibres breakage can be attributed to the inter-crystal slippage in the material. At the hooked end, the localized stresses remarkably accelerate the inter-crystal slip process. Consequently, the hook part reaches the yield condition first and fibre breakage occurs.

Fig. 10 summarizes the maximum pull-out forces of the designed UHPC matrices. It can be obtained from the figure that the ternary binder pastes (M2~M7) has a higher maximum pull-out force than that of the quaternary binder ones (M9~M14). This observation can be related to the higher compressive strength of former groups (M2~M7), resulting in a stronger fibre-matrix interface (Yoo et al., 2017). Moreover, the substitution of LP seems to have no significant or just slight fluctuation on the bond properties. On the one hand, replacing cement by LP can result in a weaker matrix strength in the interface zone due to dilution effect of reactive clinker and thus a reduced bond force; on the other hand, the enlarged shrinkage provides a confinement around the fibre (Hun et al., 2014) and formation of calcium carboaluminate

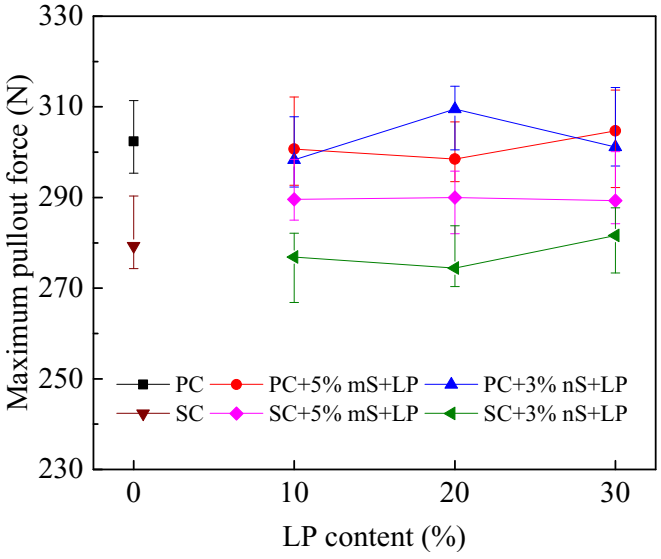

Fig. 10. Maximum pull-out force.

(Wang et al., 2018) in the presence of LP, which in turn improves the frictional resistance during the fibre pull-out. Furthermore, the filling effects of the mS or nS between the interfaces also help to compensate the bond-strength reduction due to the LP. In addition, the pozzolanic reactions of the mS and nS can further improve the fibre-matrix bond strength by replacing calcium-hydroxide crystals with higher strength calcium silicate gels in the interface zone (Wu et al., 2016). In this study, 3% nS has limited difference in bonding effect compared to 5% mS.

3.5. Total free shrinkage

The total free shrinkage is defined as the contracting of a sample due to both chemical process of hydration (autogenous shrinkage) and loss of capillary water (drying shrinkage), which is related to crack resistance and durability especially in arid and desert regions (Hu et al., 2017; W. Li et al., 2017b; Yang, 2015). Based on Mackenzie (2002) and Kelvin-Laplace equation (Bentz, 2008), the shrinkage strain is given as:

$$\varepsilon_p = \sigma_{cap}\left(\frac{1}{3K} - \frac{1}{K_s}\right) \tag{2}$$

$$\sigma_{cap} = \frac{2\gamma cos\alpha}{r} = \frac{-\ln(RH)\rho RT}{M} \tag{3}$$

where K and K_s are bulk modulus of the whole matrix and solid material, respectively. σ_{cap} is the capillary tensile stress. M and ρ are molar weight and density of water, respectively. RH is the relative humidity. R is ideal gas constant. T is absolute temperature. According to Eqs. (2) and (3), the quaternary blends effect on drying shrinkage is mainly influenced by the different abilities of capillary water loss in different mixtures. The total free shrinkages of 14 mixtures are shown in Fig. 11, ranging from about 720×10^{-6} (M1) to 1230×10^{-6} (M11).

Compared to that of PC paste, the total free shrinkage of SC paste grows faster at the first week due to more free water loss and more capillary pores between 30 nm and 50 nm (drying shrinkage) caused by dilution effect of PC clinker by GGBS. At later age, the total free shrinkage of PC paste develops faster or with a comparable rate to SC paste, probably due to higher further hydration process (autogenous shrinkage), which is in line with the strength development presented in Section 3.3. Normally, the LP generates

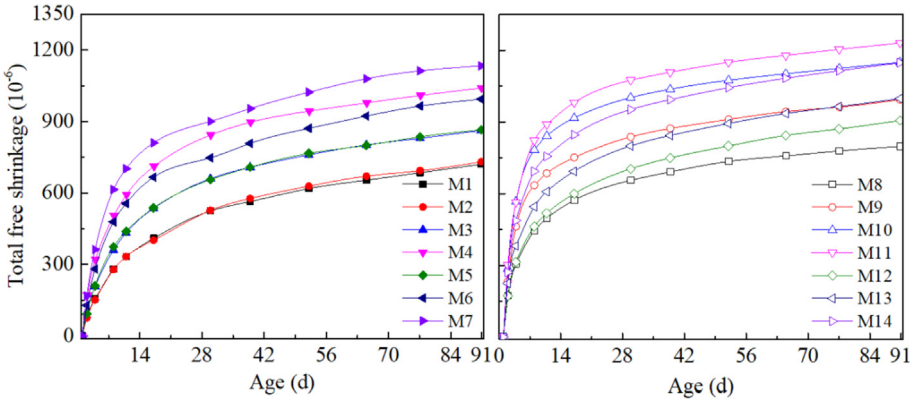

Fig. 11. Total free shrinkage of pastes.

an enlarged shrinkage due to increased water-to-clinker ratio (see Table 2) and dilution of reactive binder (illustrated in Section 3.1), which results in less hydration product to fill the small pores (see Fig. 6) and higher free water content is left in the pores. It makes the relative humidity easily loss, consequently increasing the capillary tensile stress and drying shrinkage. Hence, it is wise to apply mS or nS to restrict the shrinkage development in the presence of LP utilization, by generation of more C—S—H gel by pozzolanic reaction with calcium hydroxide and better pore structure refinement (Wongkeo et al., 2012). It is clear that, the total free shrinkages increase rather limited with relatively low LP contents under the condition of 5% mS or 3% nS addition. For example, the increase of total free shrinkages of M2, M3, M5 are 1.5%, 19.8% and 20.1%, respectively, compared with that of PC paste at the age of 91 days. While M9, M12, M13 show increase proportions of 24.5%, 13.6% and 25.1%, respectively, compared with that of SC paste at the age of 91 days. It should be noted that an addition of 5% mS is better for inhibiting the shrinkage of ternary binder mixtures (PC + mS/nS + LP), while 3% mS is better for the quaternary binder mixtures (SC + mS/nS + LP). This preferential combination of PC-mS and SC-nS is in accordance with the results of compressive strength in Section 3.3.

3.6. Environmental sustainability

Life cycle assessment (LCA) has been widely investigated and applied in construction industry to evaluate the environmental sustainability of consumer products. A small scale evaluation of materials level is appropriate to compare the different environmental sustainability of concrete mixtures (Van den Heede and De Belie, 2017). The total embedded CO_2 emission for each UHPC paste, based on 1 m^3, is first calculated including all components as,

$$m_{CO_2} = \sum_{i=1}^{i=n} r(i) \cdot m_{CO_2}(i) \quad (4)$$

where $r(i)$ represents the mass fraction of powder i, $m_{CO_2}(i)$ is the embodied CO_2 of powder i based on (King, 2012; Wang et al., 2019; Yu et al., 2015) as presented in Table 3. It should be noted that these values can vary depending on raw materials, production methods etc. (Van Den Heede and De Belie, 2012). The embedded CO_2 emissions of the 14 UHPC pastes are shown in Table 4. With the addition of 50% GGBS in SC, its embedded CO_2 emission has a significant decrease to 1092 kg/m^3, compared to the value of PC (1797 kg/m^3). The environmental sustainability is further improved with the increasing content of LP, till 731 kg/m^3 in the case of quaternary mixture of M14 with a reduction of 59% based on the pure PC.

As shown in Fig. 8 and Table 4, UHPC paste with a higher compressive strength normally corresponds to a larger embedded CO_2 emission. Hence, it is not comprehensive to evaluate the environmental sustainability by only the absolute embedded CO_2 emission. One significant importance in environmental sustainability assessment is therefore the definition of the functional unit. A good indicator is widely accepted that uses the normalized strength by CO_2 emission (Damineli et al., 2010), which is adopted in the present study, as

$$\beta = \sigma_c / m_{CO_2} \quad (5)$$

where β is the binder sustainability efficiency based on strength (MPa/(kg/m^3)), a larger value indicates a higher environmental sustainability efficiency. σ_c is the compressive strength of UHPC paste after 28 days, MPa. The binder environmental sustainability efficiencies of UHPC pastes are shown in Table 4. UHPC pastes with higher compressive strength usually have relatively lower environmental sustainability efficiency. This is linked to the relatively low hydration degree and cement efficiency when the cement

Table 3
Embedded CO_2 emission of ingredients.

Material	Portland cement	GGBS	Silica powder	Limestone powder
CO_2 emission (kg/ton)	930	52	28	32

Table 4
Embedded CO_2 emission and sustainability efficiency.

Mix	Note	CO_2 emission (kg/m^3)	(MPa/(kg/m^3))
M1	PC	1797	0.086
M2	PC5mS10LP	1505	0.095
M3	PC5mS20LP	1322	0.113
M4	PC5mS30LP	1143	0.120
M5	PC3nS10LP	1546	0.098
M6	PC3nS20LP	1362	0.114
M7	PC3nS30LP	1181	0.127
M8	SC	1092	0.134
M9	PC5mS10LP	921	0.150
M10	PC5mS20LP	814	0.165
M11	PC5mS30LP	708	0.185
M12	PC3nS10LP	945	0.163
M13	PC3nS20LP	837	0.180
M14	PC3nS30LP	731	0.198

amount is relatively high at relatively low water-to-binder ratio. With the utilization of GGBS and LP, the sustainability efficiency β is enhanced, from approximately 0.086 MP/(kg/m^3) at mixture M1 to 0.198 MP/(kg/m^3) at mixture M14, with improvement of 130%.

To sum up, the values of embedded CO_2 emission and binder efficiency of UHPC pastes with blended binders are significantly improved compared to the PC pastes, with maximum improvements of 59% reduction and 130% respectively, which means the sustainable binder with quaternary blends has a lower environmental impact and higher sustainability efficiency.

3.7. Synergy of quaternary blends

As illustrated above, the quaternary binders with cement-slag-limestone-silica can greatly reduce the embedded CO_2 emission and sustainability efficiency in UHPC system. However, it also should be noted that binders including slag or limestone powder tend to dilute Portland cement and show certain negative influence on compressive strength, fibre-to-matrix bond and total free shrinkage. It is critical to calculate synergy to quantify if there has some positive or negative combined effect in hybrid mixes (Banthia et al., 2014; Banthia and Gupta, 2004). Thus, it is important to understand if the quaternary blends show diminished or enlarged negative dilution influence. In this study, a synergy calculation method is adopted to assess the hybridization of quaternary blends compared to binary (cement-slag) and ternary binders (cement-silica-limestone), based on the following formula:

$$synergy = \frac{\left(X_{ref} - X_B\right) + \left(X_{ref} - X_T\right)}{X_{ref} - X_Q} - 1 \quad (6)$$

where X represents the properties of UHPC pastes, namely compressive strength, fibre-to-matrix bond and shrinkage in this study. To be specific, X_{ref}, X_B, X_T, X_Q are the property in reference (cement), binary binder (cement-slag), ternary binder (cement-silica-limestone) and quaternary binder (cement-slag-silica-limestone), respectively. A positive synergy (>0) indicates that quaternary blends has less adverse influence than binary and ternary blends. A negative synergy with a value between −1 and 0 represents the adverse influence is enlarged.

Fig. 12 presents the synergies in terms of 28 days compressive strengths, fibre-to-matrix bond and total free shrinkage calculated by Eq. (6). The synergy values in quaternary UHPC pastes are in general positive, except for only a few negative values. There exists positive synergy in quaternary binders to compensate the negative dilution effect, compared to binary or ternary ones. The quaternary blends probably optimize the total particle size distribution (Arora et al., 2018) and then enhance the compactness that is confirmed by the wet packing density in Fig. 7, which contributes to the positive synergy values. Furthermore, compared to the binary blends (slag cement), introducing limestone powder into the quaternary blends can increase the water-to-reactive binder ratio and improve the hydration degree of both cement and slag. Incorporating slag into ternary blends (cement-silica-limestone) tends to optimize the Ca/Si ratio. Hence, it is reasonable to develop sustainable UHPC pastes with quaternary blends instead of binary or ternary ones. In short, considering fresh and hardened properties, environmental sustainability and synergy, the quaternary binders of SC3nS10LP and SC3nS20LP are suggested for developing sustainable UHPC.

4. Conclusions

This article addresses the synergy effect of quaternary blends of cement-slag-limestone-micro/nano silica on the properties of UHPC pastes, with the aim of designing UHPC with lowered environmental impact. 14 UHPC pastes are designed by blending different proportions of Portland cement, slag cement containing 50% of GGBS, limestone powder and micro/nano silica, at a low water-to-powder ratio of 0.2. The main conclusions can be summarized:

- Quaternary blends with cement-slag-silica-limestone have considerable advantage of environmental sustainability for UHPC pastes compared to the pure Portland cement, with maximum improvements of 59% CO_2 emission reduction and 130% sustainability efficiency based on strength.
- The designed quaternary binders in general slightly accelerate the hydration process and dilute the heat flow and total heat, but significantly improves the hydration degree and efficiency of cement in UHPC pastes. Furthermore, the pore structures of

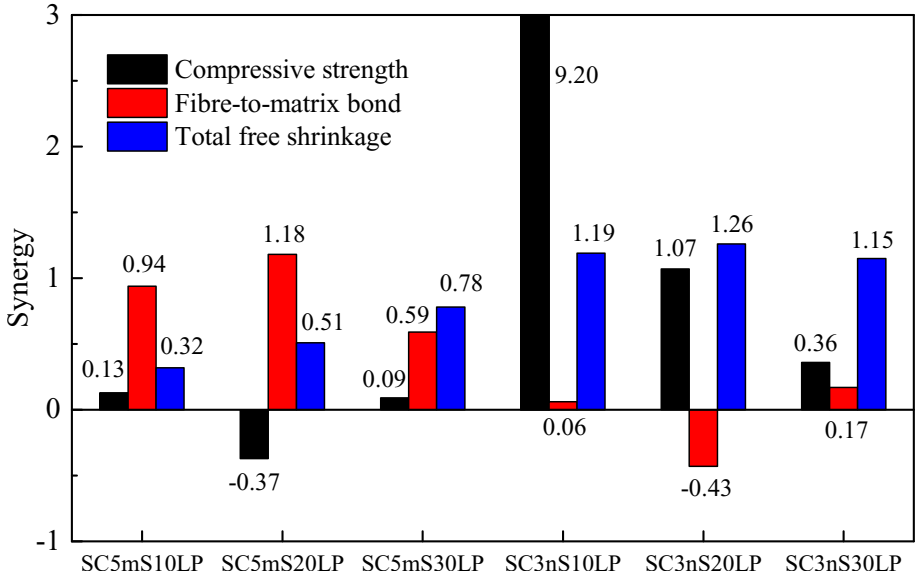

Fig. 12. Synergy of quaternary binders compared to binary and ternary ones.

UHPC pastes with quaternary binders are densified compared to the mixture with pure Portland cement.

- Limestone powder contributes to better environmental sustainability, spread flow and wet packing density, but causes enlarged total free shrinkage and diminished strength of UHPC pastes due to dilution effect, while application of silica powder is an effective counter measure to overcome those disadvantages due to nucleation, pozzolanic and filling effects.
- Slag cement possessing a relatively lower Ca/Si ratio (2.45) is preferred to a lower amount but finer silica in the presence of limestone powder to achieve enhanced hardened properties (3% nano silica for the quaternary binders), compared to the Portland cement with a higher Ca/Si (3.22) that needs more silica even with coarser particle size (5% micro silica for the ternary binders).
- Positive synergies in term of strength, fibre-to-matrix bond and total free shrinkage can be observed in UHPC pastes with quaternary binders (cement-slag-silica-limestone) compared to binary (cement-slag) and ternary (cement-silica-limestone) ones. It demonstrates the reasonability of quaternary blends for developing sustainable UHPC system instead of binary or ternary ones.

Acknowledgements

This study was funded by the China Scholarship Council and Eindhoven University of Technology. The appreciation is also expressed to the ENCI for the material support.

References

Arora, A., Aguayo, M., Hansen, H., Castro, C., Federspiel, E., Mobasher, B., Neithalath, N., 2018. Microstructural packing- and rheology-based binder selection and characterization for Ultra-high Performance Concrete (UHPC). Cement Concr. Res. 103, 179–190.
Banthia, N., Gupta, R., 2004. Hybrid fiber reinforced concrete (HyFRC): fiber synergy in high strength matrices. Mater. Struct. Constr. 37, 707–716.
Banthia, N., Majdzadeh, F., Wu, J., Bindiganavile, V., 2014. Fiber synergy in hybrid fiber reinforced concrete (HyFRC) in flexure and direct shear. Cement Concr. Compos. 48, 91–97.
Bentz, D.P., 2008. A review of early-age properties of cement-based materials. Cement Concr. Res. 38, 196–204.
Bentz, D.P., Ferraris, C.F., Jones, S.Z., Lootens, D., Zunino, F., 2017. Limestone and silica powder replacements for cement: early-age performance. Cement Concr. Compos. 78, 43–56.
Bouasker, M., Khalifa, N.E.H., Mounanga, P., Ben Kahla, N., 2014. Early-age deformation and autogenous cracking risk of slag-limestone filler-cement blended binders. Constr. Build. Mater. 55, 158–167.
Burroughs, J.F., Shannon, J., Rushing, T.S., Yi, K., Gutierrez, Q.B., Harrelson, D.W., 2017. Potential of finely ground limestone powder to benefit ultra-high performance concrete mixtures. Constr. Build. Mater. 141, 335–342.
C 307-03, 2004. Standard Test Method for Tensile Strength of Chemical-Resistant Mortar, Grouts, and Monolithic Surfacings. ASTM Stand.
Cao, Y.Y.Y., Yu, Q.L., 2018. Effect of inclination angle on hooked end steel fiber pullout behavior in ultra-high performance concrete. Compos. Struct. 201, 151–160.
Colangelo, F., Messina, F., Di Palma, L., Cioffi, R., 2017. Recycling of non-metallic automotive shredder residues and coal fly-ash in cold-bonded aggregates for sustainable concrete. Compos. B Eng. 116, 46–52.
Crossin, E., 2015. The greenhouse gas implications of using ground granulated blast furnace slag as a cement substitute. J. Clean. Prod. 95, 101–108.
Damineli, B.L., Kemeid, F.M., Aguiar, P.S., John, V.M., 2010. Measuring the eco-efficiency of cement use. Cement Concr. Compos. 32, 555–562.
Dave, N., Kumar, A., Srivastava, A., Kumar, A., Kumar, S., 2017. Study on quaternary concrete micro-structure , strength , durability considering the influence of multi-factors. Constr. Build. Mater. 139, 447–457.
Dave, N., Kumar, A., Srivastava, A., Kumar, S., 2016. Experimental analysis of strength and durability properties of quaternary cement binder and mortar. Constr. Build. Mater. 107, 117–124.
De Belie, N., Kratky, J., Van Vlierberghe, S., 2010. Influence of pozzolans and slag on the microstructure of partially carbonated cement paste by means of water vapour and nitrogen sorption experiments and BET calculations. Cement Concr. Res. 40, 1723–1733.
DIN 52-450, 1985. Determination of Shrinkage and Expansion of small test specimens. Ger. Stand.
Domone, P., Hsi-wen, C., 1997. Testing of binders for high performance concrete. Cement Concr. Res. 27, 1141–1147.
Edwin, R.S., De Schepper, M., Gruyaert, E., De Belie, N., 2016. Effect of secondary copper slag as cementitious material in ultra-high performance mortar. Constr. Build. Mater. 119, 31–44.
Edwin, R.S., Mushthofa, M., Gruyaert, E., De Belie, N., 2019. Quantitative analysis on porosity of reactive powder concrete based on automated analysis of backscattered-electron images. Cement Concr. Compos. 96, 1–10.
EFNARC, 2005. Specification and guidelines for self-compacting concrete. Rep. from EFNARC 44, 32.
El-chabib, H., Ibrahim, A., 2013. The performance of high-strength flowable concrete made with binary , ternary , or quaternary binder in hot climate. Constr. Build. Mater. 47, 245–253.
EN-1097-3, 1998. Tests for mechanical and physical properties of aggregates- Part 3: determination of loose bulk density and voids. Br. Stand. Institution-BSI CEN Eur. Comm. Stand.
EN 12390-3, 2009. Testing hardened concrete Part - 3: compressive strength of test specimens. Br. Stand. Institution-BSI CEN Eur. Comm. Stand.
Gholampour, A., Ozbakkaloglu, T., 2017. Performance of sustainable concretes containing very high volume Class-F fly ash and ground granulated blast furnace slag. J. Clean. Prod. 162, 1407–1417.
Hendriks, C.A., Worrell, E., Jager, D.de, Blok, K., Riemer, P., 2002. Emission reduction of greenhouse gases from the cement industry. Int. Energy Agency 1–11.
Hong, S.Y., Glasser, F.P., 2004. Phase relations in the CaO-SiO2-H2O system to 200 °C at saturated steam pressure. Cement Concr. Res. 34, 1529–1534.
Hosseini, P., Booshehrian, A., Madari, A., 2011. Developing concrete recycling strategies by utilization of nano-SiO2 particles. Waste and Biomass Valorization 2, 347–355.
Hu, X., Shi, Z., Shi, C., Wu, Z., Tong, B., Ou, Z., de Schutter, G., 2017. Drying shrinkage and cracking resistance of concrete made with ternary cementitious components. Constr. Build. Mater. 149, 406–415.
Hun, S., Sung, G., Taek, K., Joo, D., 2014. Effect of shrinkage reducing agent on pullout resistance of high-strength steel fibers embedded in ultra-high-performance concrete. Cement Concr. Compos. 49, 59–69.
Kakali, G., Tsivilis, S., Aggeli, E., Bati, M., 2000. Hydration products of C3A, C3S and Portland cement in the presence of CaCO3. Cement Concr. Res. 30, 1073–1077.
King, D., 2012. The effect of silica fume on the properties of concrete as defined in concrete society report 74, cementitious materials. 37th Conf. Our world Concr. Struct. 1–23.
Koutný, O., Snoeck, D., Van Der Vurst, F., De Belie, N., 2018. Rheological behaviour of ultra-high performance cementitious composites containing high amounts of silica fume. Cement Concr. Compos. 88, 29–40.
Lei, D.Y., Guo, L.P., Sun, W., Liu, J., Shu, X., Guo, X.L., 2016. A new dispersing method on silica fume and its influence on the performance of cement-based materials. Constr. Build. Mater. 115, 716–726.
Li, L.G., Kwan, A.K.H., 2014. Packing density of concrete mix under dry and wet conditions. Powder Technol. 253, 514–521.
Li, P.P., Yu, Q.L., 2019. Responses and post-impact properties of ultra-high performance fibre reinforced concrete under pendulum impact. Compos. Struct. 208, 806–815.
Li, P.P., Yu, Q.L., Brouwers, H.J.H., 2018. Effect of coarse basalt aggregates on the properties of Ultra-high Performance Concrete (UHPC). Constr. Build. Mater. 170, 649–659.
Li, P.P., Yu, Q.L., Brouwers, H.J.H., 2017a. Effect of PCE-type superplasticizer on early-age behaviour of ultra-high performance concrete (UHPC). Constr. Build. Mater. 153.
Li, W., Huang, Z., Hu, G., Hui Duan, W., Shah, S.P., 2017b. Early-age shrinkage development of ultra-high-performance concrete under heat curing treatment. Constr. Build. Mater. 131, 767–774.
Li, W., Huang, Z., Zu, T., Shi, C., Duan, W.H., Shah, S.P., 2015. Influence of nano-limestone on the hydration, mechanical strength, and autogenous shrinkage of ultrahigh-performance concrete. J. Mater. Civ. Eng. 28, 04015068.
Mackenzie, J.K., 2002. The elastic constants of a solid containing spherical holes. Proc. Phys. Soc. Sect. B 63, 2–11.
Makhloufi, Z., Aggoun, S., Benabed, B., Kadri, E.H., Bederina, M., 2016. Effect of magnesium sulfate on the durability of limestone mortars based on quaternary blended cements. Cement Concr. Compos. 65, 186–199.
Makhloufi, Z., Bouziani, T., Hadjoudja, M., Bederina, M., 2014. Durability of limestone mortars based on quaternary binders subjected to sulfuric acid using drying – immersion cycles. Constr. Build. Mater. 71, 579–588.
Mo, K.H., Chin, T.S., Alengaram, U.J., Jumaat, M.Z., 2016. Material and structural properties of waste-oil palm shell concrete incorporating ground granulated blast-furnace slag reinforced with low-volume steel fibres. J. Clean. Prod. 133, 414–426.
Nili, M., Ehsani, A., 2015. Investigating the effect of the cement paste and transition zone on strength development of concrete containing nanosilica and silica fume. Mater. Des. 75, 174–183.
Pedro, D., Brito, J.De, Evangelista, L., 2017. Mechanical characterization of high performance concrete prepared with recycled aggregates and silica fume from precast industry. J. Clean. Prod. 164, 939–949.
Robins, P., Austin, S., Jones, P., 2002. Pull-out behaviour of hooked steel fibres. Mater. Struct. 35, 434–442.
Schröfl, C., Gruber, M., Plank, J., 2012. Preferential adsorption of polycarboxylate superplasticizers on cement and silica fume in ultra-high performance concrete (UHPC). Cement Concr. Res. 42, 1401–1408.

Sekkal, W., Zaoui, A., 2013. Nanoscale analysis of the morphology and surface stability of calcium carbonate polymorphs. Sci. Rep. 3, 1587.
Sharma, R., Khan, R.A., 2017. Sustainable use of copper slag in self compacting concrete containing supplementary cementitious materials. J. Clean. Prod. 151, 179–192.
Shi, C., Wang, D., Wu, L., Wu, Z., 2015. The hydration and microstructure of ultra high-strength concrete with cement–silica fume–slag binder. Cement Concr. Compos. 61, 44–52.
Stengel, T., Schießl, P., 2014. Life Cycle Assessment (LCA) of Ultra High Performance Concrete (UHPC) Structures, Eco-Efficient Construction and Building Materials. Woodhead Publishing Limited.
Su, Y., Wu, C., Li, J., Li, Z.X., Li, W., 2017. Development of novel ultra-high performance concrete: from material to structure. Constr. Build. Mater. 135, 517–528.
Van den Heede, P., De Belie, N., 2017. 9 - sustainability assessment of potentially 'green' concrete types using life cycle assessment. In: Savastano Junior, H., Fiorelli, J., Dos Santos, S.F.B.T.-S. And N.C.M. Using I.B.F.C. Woodhead Publishing, pp. 235–263.
Van den Heede, P., De Belie, N., 2014. A service life based global warming potential for high-volume fly ash concrete exposed to carbonation. Constr. Build. Mater. 55, 183–193.
Van Den Heede, P., De Belie, N., 2012. Environmental impact and life cycle assessment (LCA) of traditional and "green" concretes: literature review and theoretical calculations. Cement Concr. Compos. 34, 431–442.
Vance, K., Aguayo, M., Oey, T., Sant, G., Neithalath, N., 2013. Hydration and strength development in ternary portland cement blends containing limestone and fly ash or metakaolin. Cement Concr. Compos. 39, 93–103.
Wang, D., Shi, C., Farzadnia, N., Shi, Z., Jia, H., 2018. A review on effects of limestone powder on the properties of concrete. Constr. Build. Mater. 192, 153–166.
Wang, W., Liu, J., Agostini, F., Davy, C.A., Skoczylas, F., Corvez, D., 2014. Durability of an ultra high performance fiber reinforced concrete (UHPFRC) under progressive aging. Cement Concr. Res. 55, 1–13.
Wang, Y., Shui, Z., Gao, X., Huang, Y., Yu, R., Li, X., Yang, R., 2019. Utilizing coral waste and metakaolin to produce eco-friendly marine mortar: hydration, mechanical properties and durability. J. Clean. Prod. 219, 763–774.
Wongkeo, W., Thongsanitgarn, P., Chaipanich, A., 2012. Compressive strength and drying shrinkage of fly ash-bottom ash-silica fume multi-blended cement mortars. Mater. Des. 36, 655–662.
Wu, Z., Shi, C., Khayat, K.H., 2016. Influence of silica fume content on microstructure development and bond to steel fiber in ultra-high strength cement-based materials (UHSC). Cement Concr. Compos. 71, 97–109.
Yajun, J., Cahyadi, J.H., 2003. Effects of densified silica fume on microstructure and compressive strength of blended cement pastes. Cement Concr. Res. 33, 1543–1548.
Yang, W., 2015. Fatal factor for durability: drying shrinkage. In: The Issues and Discussion of Modern Concrete Science. Springer, Berlin, Heidelberg.
Yazici, H., Yiğiter, H., Karabulut, A.Ş., Baradan, B., 2008. Utilization of fly ash and ground granulated blast furnace slag as an alternative silica source in reactive powder concrete. Fuel 87, 2401–2407.
Yoo, D., Park, J., Kim, S., 2017. Fiber pullout behavior of HPFRCC : effects of matrix strength and fiber type. Compos. Struct. 174, 263–276.
Yu, R., Song, Q., Wang, X., Zhang, Z., Shui, Z., Brouwers, H.J.H., 2017. Sustainable development of Ultra-High Performance Fibre Reinforced Concrete (UHPFRC): towards to an optimized concrete matrix and efficient fibre application. J. Clean. Prod. 162, 220–233.
Yu, R., Spiesz, P., Brouwers, H.J.H., 2015. Development of an eco-friendly Ultra-High Performance Concrete (UHPC) with efficient cement and mineral admixtures uses. Cement Concr. Compos. 55, 383–394.
Yu, R., Spiesz, P., Brouwers, H.J.H., 2014a. Mix design and properties assessment of ultra-high performance fibre reinforced concrete (UHPFRC). Cement Concr. Res. 56, 29–39.
Yu, R., Spiesz, P., Brouwers, H.J.H., 2014b. Effect of nano-silica on the hydration and microstructure development of Ultra-High Performance Concrete (UHPC) with a low binder amount. Constr. Build. Mater. 65, 140–150.
Zhong, R., Wille, K., Viegas, R., 2018. Material efficiency in the design of UHPC paste from a life cycle point of view. Constr. Build. Mater. 160, 505–513.